JOURNAL OF MATERIALS SCIENCE 22 (1987) 3907–3916

Characterizing the surface contact behaviour of ceramics

Part 1 *Hardness response of glass-bonded alumina and titania*

J. T. CZERNUSZKA*, T. F. PAGE‡,
Department of Metallurgy and Materials Science, University of Cambridge, Pembroke Street, Cambridge CB2 3QZ, UK

The indentation hardness of four glass-bonded ceramics has been examined as a function of load and temperature. It has been observed that the relative hardness values may interchange depending on the temperature and load of testing. For each material there are two regimes of temperature dependence. It has been possible to qualitatively correlate the transition temperature with the composition of the glassy binder phase.

1. Introduction

Ceramic materials are increasingly being employed in applications where good wear and erosion resistance is required, often at high temperatures and in chemically hostile environments. To optimise materials' properties for these uses, a knowledge of how various ceramics respond to surface contacts is necessary. Thus, an understanding of how the resultant deformation depends on load (and thus, contact scale), microstructure, temperature and chemical environment will be important in assessing a material's suitability for application in a particular wear situation.

Surface contacts in brittle materials generally result in a combination of plastic flow and localized fracture, both of which may also be observed around hardness impressions. While plastic flow is always observed as being the principle deformation mechanism accommodating the indentor shape, localized indentation fracture is only observed above a critical load, depending upon material and microstructure, etc. Hence the hardness test is ideally suited as a convenient means of examining the near-surface plasticity and fracture behaviour of ceramics in a carefully controlled and reproducible manner. Indeed, indentation hardness is often used as a selection parameter for ranking the wear resistance of materials. This inferred relationship between hardness and wear arises from the suggestion that an abrasive asperity or wear particle is similar to an indentor penetrating and ploughing through a surface. There is confirmation of this approach for many elemental metals [1]. However, although similar deformation mechanisms have been observed beneath indentations and worn surfaces of ceramics [2–4], there is apparently no such simple connection. This is due to a number of causes, including:

(i) surface contacts may also involve localized fracture, which may result in rapid material removal (e.g. [5]);

(ii) microhardness is not a material constant and is well-established to be sensitive to contact size and temperature [6–8];

(iii) environmental effects (e.g. [9]);

(iv) the stress distributions in quasi-static hardness tests and sliding contacts are significantly different and will include factors due to indenter shape, strain rate and friction (e.g. [10]);

(v) more complex wear mechanisms involving chemical reactions, phase transformations, fatigue, etc., may occur (e.g. [11]).

The work described here results from an extensive study [12, 13] of the surface deformation and wear behaviour of a range of ceramics potentially useful as wear-resistant surfaces (for example, textile thread guides) under conditions where indentation fracture is not believed to play any significant role. Thus, factors (ii) and (iii) above have been of primary interest. This paper describes the contact size and temperature sensitivity of the indentation hardness of a range of glass-bonded aluminas and a glass-bonded titania. Companion papers will describe environmental effects for these materials and similar observations for a range of alloyed zirconias.

Some observations of various wear mechanisms in these materials have already been published [11, 14, 15] and future papers will address the overall wear mechanisms and wear rates observed in these materials under various conditions.

2. Materials and characterization

The materials chosen for this study were three alumina-based and one titania-based glass-bonded ceramics, themselves used as wear-resistant surfaces in the textile industry. Sections were cut from cylindrical samples (~4.7 mm diameter) with a Capco Q35 diamond saw and polished on a series of diamond-loaded laps and cloths. The polishing methods are fully described in [13], but essentially comprised a sequence from 14 μm diamond paste on a cast iron lap to 0.25 μm

* *Present address*: Department of Metallurgy and Science of Materials, University of Oxford, Parks Road, Oxford, UK.
‡ *Present address*: Department of Metallurgy and Engineering Materials, University of Newcastle Upon Tyne, Newcastle Upon Tyne, NE1 7RU, UK.

0022–2461/87 $03.00 + .12

TABLE I Microstructural characterization

	Material			
	HX	RG	FW	TE
Grain size (μm)	~5 (1–10)	~4.5 (1–10)	~15 (5–40)	~1.5 (0.5–3)
Crystalline phase (%)	70	75	85	~90
Glassy phase (%)	20	15	8	<5
Porosity (%)	10	10	7	<5
Density ($g\,cm^{-3}$)	3.2	3.45	3.7	4.1

diamond paste on a napp-free cloth. Polishing was continued until the surfaces were free from obvious scratches and porosity from damaged grains. After hardness testing, specimens were gold coated and examined by scanning electron microscopy (SEM). Back-scattered electron (BSE) imaging using a four-quadrant silicon detector in a Camscan 4 SEM allowed the grains to be distinguished from the second glassy binder phase by atomic number contrast [11]. Representative micrographs are shown in Fig. 1 and from sequences of similar photographs grain-size distributions and phase proportions were determined (Table I). Chemical compositions of the two phases were determined by energy dispersive X-ray microanalysis (EDX) using a Link 860 Mk2 system on an ISI 100A SEM. In this case the specimens were carbon coated. Averages of at least six readings are given in Table II, from which the binding phase can be seen to be silica-based in all cases.

3. Experimental procedure

For experiments performed under ambient laboratory conditions, a Leitz Miniload micro-hardness tester was used over the load range 5 to 1000 g, with a constant indentor dwell time of 15 sec. The temperature-variant hardness experiments were carried out in a Wilberforce Scientific Developments high-temperature hardness machine, detailed operation of which is described elsewhere [16]. Briefly, it consisted of an evacuated chamber ($< 10^{-6}$ torr) and separate furnace assemblies for the indentor and specimen, such that thermal shock effects were avoided by matching the temperatures of the indentor and the substrate. Loads of 100 to 1000 g, again at a constant indentor dwell time of 15 sec, were used. In all cases, at least five indentations were made at each load at each temperature.

4 Results

4.1. Size effects on hardness under ambient conditions

The results of the load-variant hardness behaviour are presented in Fig. 2a. For all four materials, the hardness increases with decreasing load, i.e. decreasing contact size. Fig. 2b plots the same data but as a hardness dependence on identation diagonal; similar behaviour is observed. The variation in hardness with load/diagonal is unique to each material, such that, although HX and TE have similar hardness values at large loads, at the lowest loads the hardness of HX now approaches that of RG. This type of behaviour has been previously recognized and investigated [6, 17]. The approach was to start with an equation of

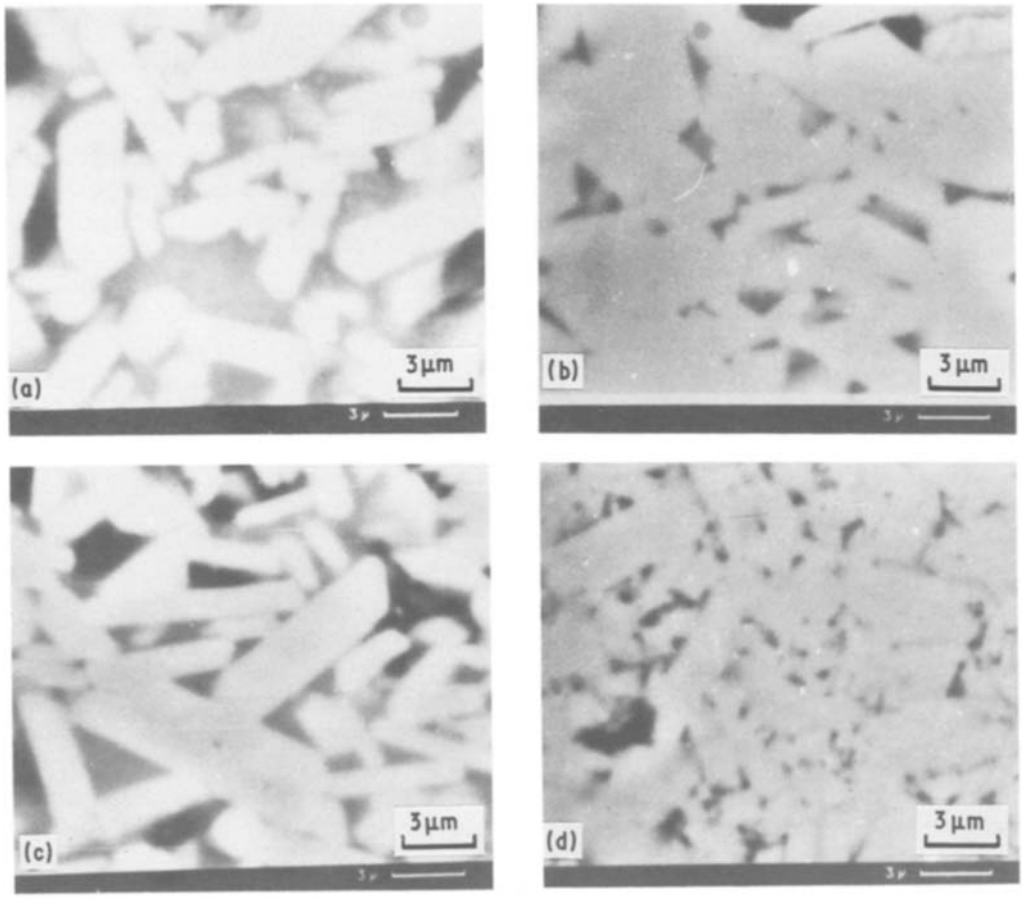

Figure 1 Back-scattered electron SEM images of (a) HX, (b) RG, (c) FW and (d) TE.

TABLE II Results of X-ray micro-analysis

	Material											
	HX			RG			FW			TE		
	g	gb	a	g	gb	a	g	gb	a	g	gb	a
Al_2O_3	89.1	50.6	73.6	86.7	81.9	87.2	97.4	94.1	99.3	2.1	4.7	3.3
TiO_2	–	–	0.4	0.2	0.4	0.1	–	–	–	96.1	92.3	93.4
SiO_2	9.1	38.5	17.1	–	12.6	6.9	2.1	4.2	0.1	0.7	2.0	2.2
CaO	0.5	6.0	2.3	1.2	1.2	2.2	–	0.2	–	0.4	0.4	0.1
MgO	0.8	1.8	2.1	3.3	3.3	1.3	0.8	1.0	0.4	0.4	0.4	0.2

g = Crystalline phase, gb = grain-boundary phase, a = average bulk composition from [15].

the type originally proposed by Meyer [18] to describe the load variation of hardness observed with spherical indentors, i.e.

$$L = ka^n \quad (1)$$

where L is the load, k a constant, a the indentation radius and n the Meyer, or more generally, the indentation size effect (ISE) index. Because hardness is proportional to a^{-2}, a value of $n = 2$ implies a load-invariant hardness. For $n < 2$, the hardness will increase with decreasing load. The constant, k, may be given to be the hardness at a given diagonal (in this case 10 μm) (e.g. [6]). The two parameters, n and $H_{10\,\mu m}$, are given in Table III and may be used to characterize the load : hardness curves over a limited load range. Also, the hardness at any given contact size may be computed (for example, the small contact sizes usually encountered in wear). It should be pointed out, however, that at shallow penetrations not only may hardness data be unreliable (through errors of measurement), but also environmental factors may significantly alter these curves [8]. Thus, HX possesses a lower ISE index than either TE or RG, i.e. its hardness is more load/diagonal dependent. The use of hardness : diagonal plots also allows the effect of microstructure on the hardness response to be readily ascertained, for example to explore any variation in hardness response as constant sized indentation affected volumes become of the order of the grain size.

4.2. Temperature-variant hardness

Fig. 3 shows the variation of hardness with indentation diagonal over a range of temperatures for HX. The curves have been fitted to Equation 1 [6]. Also included are the values of hardness at the lowest loads used (100 g). Not only does the hardness decrease with increasing temperature (at all loads), but the size dependence decreases. Similar experiments were performed for the other materials. From such data it is possible to obtain: (i) the temperature variation of hardness at a particular load (chosen as 1 kg in Fig. 4a); (ii) the variation of hardness at a constant indentation diagonal ($H_{10\,\mu m}$ is plotted in Fig. 4b); (iii) the variation of the ISE index with temperature (Fig. 5).

From Fig. 4a, it can be seen that hardness decreases with increasing temperature such that, for all cases, it falls to less than half the corresponding room-temperature value at 1000° C. For FW and TE, there is an almost linear decrease with temperature over the whole temperature range, while for HX and RG linearity is only maintained up to ~ 800° C, when the

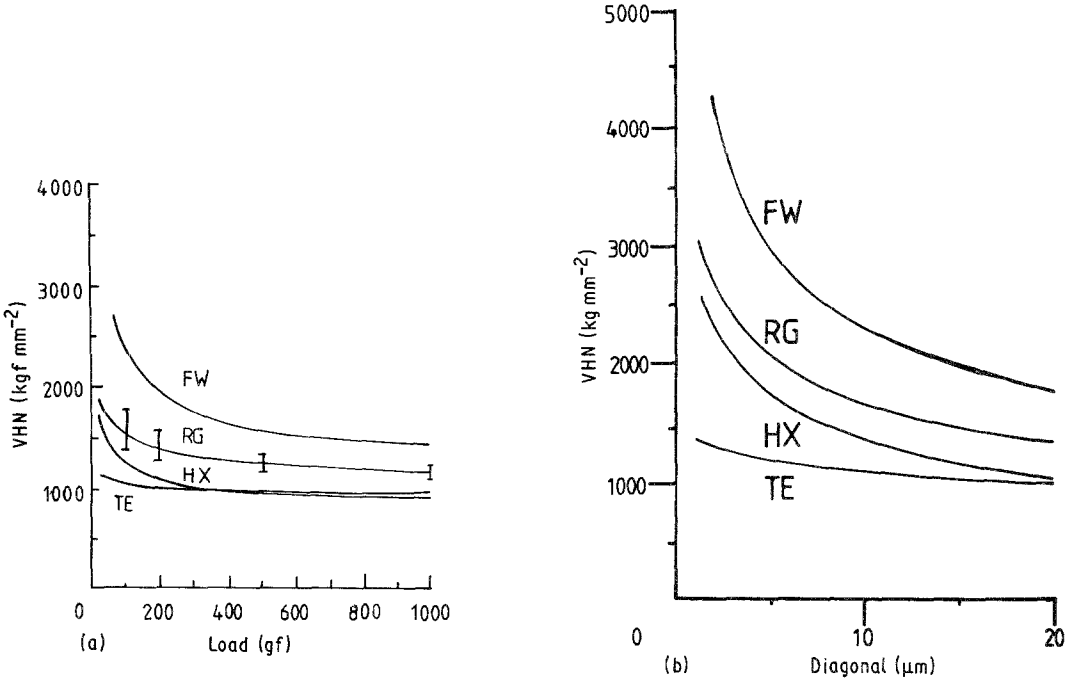

Figure 2 Plots of Vickers hardness as a function of (a) load and (b) indentation diagonal. Curves are best fits to Equation 1. Bars are one standard deviation.

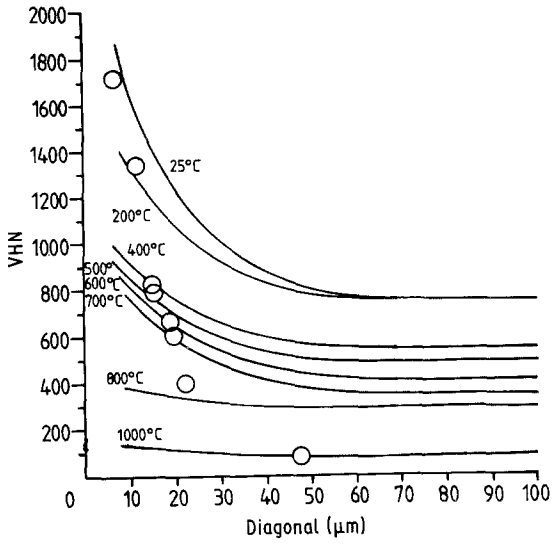

Figure 3 Plots of Vickers hardness against indentation diagonal over a range of temperatures for HX. Circles denote values for 100 g indentations. The curves have been fitted to Equation 1.

hardness of RG remains approximately constant, but that for HX drops markedly. In fact, it is only at this latter temperature that the values of TE and HX differ to any significant extent. Note that the ranking of materials by hardness values at 900° C is different to that at room temperature.

If hardness at a constant indentation diagonal against temperature is examined (Fig. 4b), then somewhat different behaviour is obtained. The hardness of FW decreases sharply and possesses the lowest hardness at ~600° C, but a similar value to RG at higher temperatures. HX and RG closely follow each other (except that HX is now harder than RG, cf. Fig. 4a) until at just over 600° C the hardness of HX is rapidly reduced and begins to follow that of TE. Note again that the relative ranking of the hardness values is also highly temperature dependent and establishes the

TABLE III Hardness at an indentation diagonal of 10 μm, $H_{10\mu m}$, and ISE

Material	$H_{10\mu m} \pm 3\sigma$	ISE index $\pm 3\sigma$
HX	1374 ± 371	1.67 ± 0.08
RG	1358 ± 637	1.73
FW	2234 ± 610	1.62
TE	1086 ± 125	1.90

importance of ascertaining hardness at the correct service temperature. Further, while the 1 kg hardness values are within the high-load plateaux of Fig. 3 (i.e. hardness insensitive to load), the hardness ranking is very size sensitive around the 10 μm value. Thus, there is clearly a need to establish hardness values at the correct conditions of both temperature and size.

A further advantage of choosing hardness at a constant diagonal, rather than constant load, is that the growth of the plastic zone surrounding the constant size indentation may be investigated (for example, by relating hardness to plastic zone size by the model of Hill [19]). By contrast, at constant load, both the diagonal and plastic zone size will increase with temperature.

The ISE: temperature behaviour is also unique to each material (Fig. 5). For HX, the initially low value rapidly tends towards 2 (the load-invariant case) above 200° C. The values for RG are almost temperature insensitive. The ISE index increases monotonically with temperature for FW until at ~600° C it attains a maximum. For TE, n tends towards 2 with increasing temperature and becomes even greater at 1000° C; i.e. hardness now decreases with decreasing load.

Another potentially useful way of extracting information from hardness: temperature data is by plotting the results as $\ln(H)$ against the reciprocal of temperature to derive an "activation energy", Q, assuming an Arrhenius equation

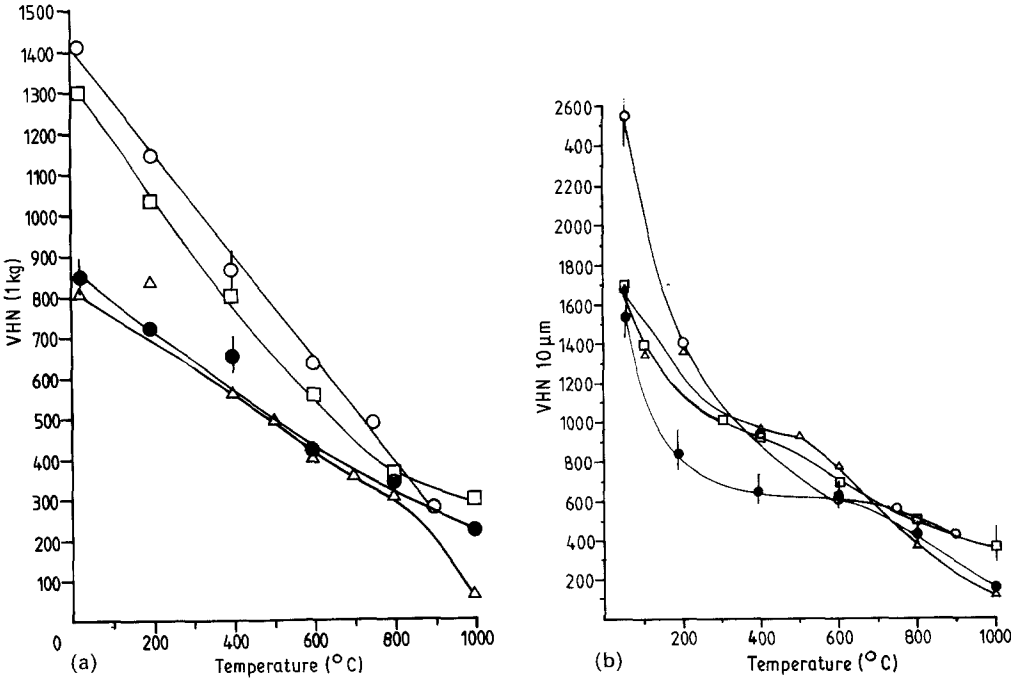

Figure 4 Temperature variation of Vickers hardness measured at (a) a load of 1 kg and (b) an indentation diagonal of 10 μm. Bars are one standard deviation. (△) HX, (□) RG, (○) FW, (●) TE.

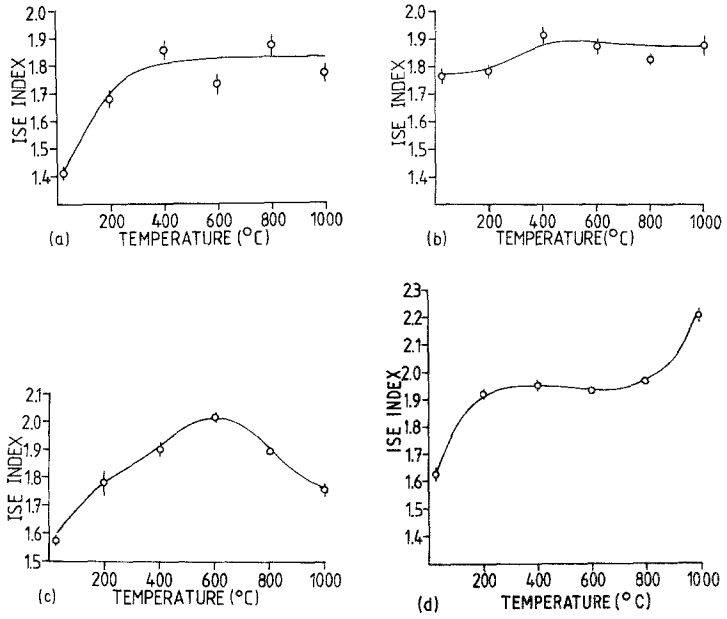

Figure 5 Plots of the variation of ISE index with temperature for (a) HX, (b) RG, (c) FW and (d) TE. Bars are one standard deviation.

$$H = H' \exp(Q/mRT) \quad (2)$$

where H' is a constant and m the creep exponent in the creep strain rate : stress relation [20, 21]. The activation energy term has been suggested to be that of the main plastic flow mechanism operating over the particular temperature range studied [21, 22] and this, in principle, may allow the deformation mechanism to be identified [23]. However, given the uncertainties in m for indentation creep, the values for Q are rarely sufficiently reliable for any definite identification to be made. Figs 6a and b present such plots using both sets of hardness values. Activation energies derived from these plots (and assuming $m = 10$, (e.g. [24])) are presented in Table IV; Q_1 and Q_2 are for the low- and high-temperature regimes, respectively. Values for various diffusion-controlled mechanisms from [23] are included for comparison.

The curves exhibit the general trend observed by other workers (e.g. [21]); at low temperatures hardness is a weak function of temperature, but above a critical temperature, T_c, the hardness is more strongly temperature sensitive. From Fig. 6a there does not appear

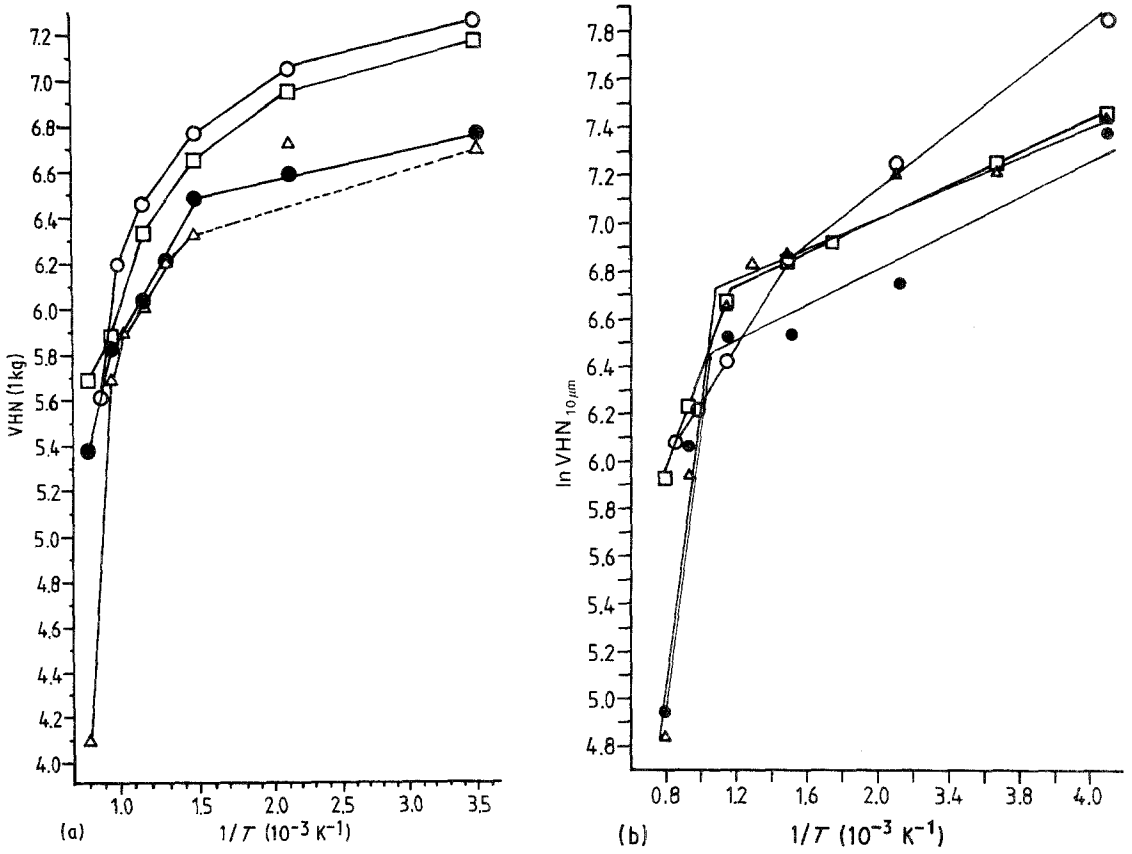

Figure 6 Plots of logarithm of Vickers hardness against reciprocal of temperature at (a) a load of 1 kg and (b) an indentation diagonal of 10 μm. Bars are one standard deviation. (○) FW, (□) RG, (△) HX, (●) TE.

TABLE IV Activation energies and critical temperatures

Material	Condition	T_c(K)	Q_1(kJ mol^{-1})	Q_2(kJ mol^{-1})
HX	1 kg	–	30.2	902.4
	10 μm	917	28.4	703.9
RG	1 kg	–	29.4	150.3
	10 μm	848	31.6	183.8
FW	1 kg	–	23.3	392.4
	10 μm	673	44.2	101.0
TE	1 kg	–	21.1	255.4
	10 μm	1031	33.8	630.9

Lattice diffusion: O^{2-} 636 kJ mol^{-1} [23]; Al^{3+} 477 kJ mol^{-1} [23].
Boundary diffusion: O^{2-} 380 kJ mol^{-1} [23]; Al^{3+} 419 kJ mol^{-1} [23].

to be a sudden transition temperature for the constant load plots, but there is a sharp value for the constant diagonal plots of Fig. 6b. This latter value is tabulated in Table IV. The value of T_c is different for each material and increases in the order: FW, RG, HX, TE.

5. Discussion

5.1. ISE behaviour

The load-variant hardness behaviour under ambient conditions (Fig. 2) is similar to that obtained on these and other two-phase ceramics [12]. It has been suggested [12] that the increase in hardness with decreasing load was due to a transition from polycrystalline to a pseudo-single-crystal behaviour. This agrees qualitatively with the grain-size determinations of Table I, i.e. materials with a larger grain size have a more pronounced ISE. For example, FW, with the largest grain size at $\sim 15\,\mu$m, possesses the largest deviation from 2 at 1.63. TE, on the other hand, with the smallest grain size, possesses the least load-variance, i.e. $n = 1.9$.

To examine this possibility, an SEM examination of the indentations was performed. Fig. 7 shows micrographs of Vickers indentations produced at loads of 1 kg and 100 kg in HX. At both loads both microstructural phases are encountered by the indentation. So, the ISE cannot be due solely to a simple grain-size effect, though the influence of microstructural scale on the plastic zone size is presumably strong [6, 25]. From measurements, it appears that the shape of both indentations is similar, i.e. no difference in gross elastic recovery appears to exist. So this effect is also not a major cause of the ISE. Other possible mechanisms include surface effects, the curvature of dislocation loops and slip inter-penetration (e.g. [6]); these have not been investigated in this study. Clearly, further understanding of these, and possibly other, effects must await more detailed knowledge of the deformation mechanisms operating beneath the indentor and the way in which the free surface modifies this deformation. Even so, the ISE behaviour may still be useful as a means of "materials characterization".

5.2. Variation of the ISE index with temperature and environment

From Fig. 3, it is clear that the lowest loads used in these experiments created an impression just less than 10 μm wide at room temperature. However, as the temperature is progressively increased, the amount of extrapolation required becomes steadily more extensive. The ISE approach is only strictly valid over the size range at which it can be directly measured [17]. So, the extrapolated values calculated and plotted in Figs 4b and 6b should be treated with some caution. Moreover, $H_{10\,\mu m}$ values lie in the range where the rate of change of hardness with diagonal is increasing, so the values of Fig. 4b show the superposition of the temperature dependence of hardness and ISE index. Thus, it seems likely that the difference in behaviour between Figs 4a and b can be accounted for, in part, by this extra factor. It also seems reasonable that the changing hardness rankings with temperature in Fig. 4b is further due in part to the ISE index being different for each material at each temperature (see Fig. 5).

The variation of ISE index with temperature for HX (Fig. 5a) is quite typical of many ceramics [21] and is thought to arise from the plastic zone around the indentation becoming large with respect to both microstructural scale and the indentation itself, i.e. a "macrohardness' situation is reached even at low loads. A similar mechanism may also apply to the behaviour of FW (Fig. 5c) and TE (Fig. 5d) up to $\sim 600°$ C. The reasons why the ISE behaviour of RG (Fig. 5b) is athermal are not yet understood, but it was not pronounced even at room temperature. An explanation for why the ISE index of FW should veer away from 2 at the higher temperatures is also unavailable, but could be due to the behaviour of either the crystalline phase or the glass. The behaviour of TE at 1000° C, with $n > 2$, may be accounted for by a strain-hardening mechanism in a similar manner to annealed metals (e.g. [26]). This is not too unreason-

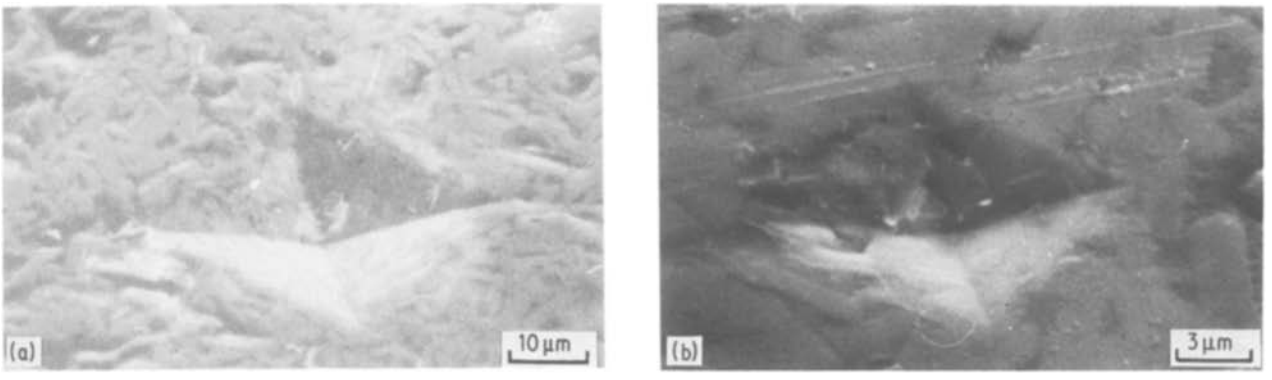

Figure 7 SE mode SEM images of Vickers indentations in HX made under ambient conditions at loads of (a) 1 kg and (b) 100 g (30 keV, 45° tilt).

able, given that half the melting temperature of rutile (the crystal form of this particular titania) has been surpassed. With $n > 2$, the sample shows a "softening" with decreasing contact size.

Incidentally, it is worth noting that for all materials (except possibly RG) the ISE is more pronounced under vacuum at room temperature (Fig. 6) than under ambient conditions (Fig. 2b and Table III). This may be attributed to environmental softening of the near-surface region (e.g. [8, 27]).

However reliable the ISE data may or may not be when extrapolated beyond our measurement range, we feel it clearly established that the changing materials' response (i.e. hardening or softening) with decreasing contact scale is an important parameter for consideration when ranking materials by hardness. Further, this ISE behaviour is sensitive to microstructure, temperature and environment.

5.3. Temperature variation of hardness

From Table IV, there seems to be no obvious correlation between the range of values for Q_1 and Q_2 with specific diffusion-controlled processes. This is perhaps not too surprising, given that the quoted data [23] were obtained on single-phase materials. In our materials, a range of processes may be occurring, including densification of the grain-boundary amorphous phase at room temperature [28], flow of this same phase at high temperatures, dislocation glide and climb in the crystalline phase. Furthermore, though in keeping with other workers we have used a value of 10 for the creep exponent m, this parameter requires laborious experimental determination for each material/temperature combination by identation (rather than bulk) creep methods. However, whatever the low-temperature and high-temperature deformation controlling mechanisms may be, we have clearly demonstrated the critical influence of temperature on hardness and hardness ranking.

Microstructural and chemical effects may be important in determining the hardness : temperature response. This will now be demonstrated in relation to the values for T_c (see Fig. 6 and Table IV). It was initially surprising that, for the aluminas, T_c should increase with decreasing alumina content (see Table I). But, on examining the chemical compositions of the glassy phase (Table II), it is evident that HX contains more silica in its grain-boundary phase than the other materials. In fact, the proportion of silica in this second phase increases in the order FW, RG, HX; the proportions of modifying and intermediate oxides is in the reverse order. Thus, the difference in T_c between the three aluminas agrees qualitatively with the proportion of network modifiers in the grain-boundary phase. This conclusively shows the importance of grain-boundary processes on the high-temperature behaviour of glass-bonded ceramics.

In order to determine whether increasing the temperature caused any differences in the deformation associated with indentation, they were examined by SEM using BSE, secondary electron (SE) and cathodoluminescence (CL) modes, including stereo-imaging. Figs 8 to 10 present examples of these high-temperature identations.

Fig. 8 presents complementary SE, BSE and stereo images in the SE mode of HX indented at 800° C. In Figs 8a and b a corner of the 1 kg Vickers indentation is visible at the top left-hand corner. A solitary crack is observed in Fig. 8a which has a meandering trajectory. The use of atomic number contrast BSE imaging in Fig. 8b shows the crack to deviate around the grains and remain mainly in the amorphous second phase. In passing, this provides an ideal example of the use of indentation techniques in examining preferential fracture paths. Because little or no fracture was observed on indenting this specimen at room temperature, the

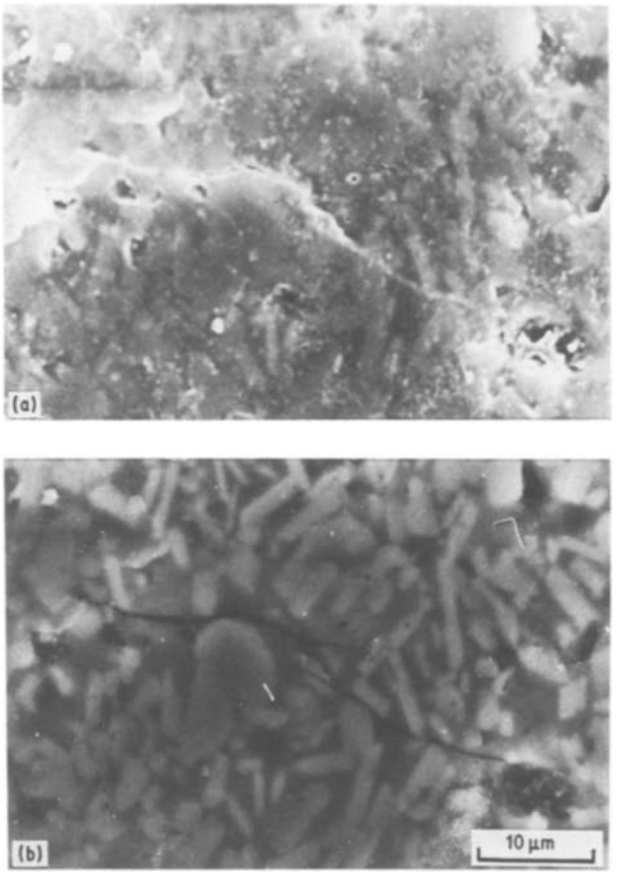

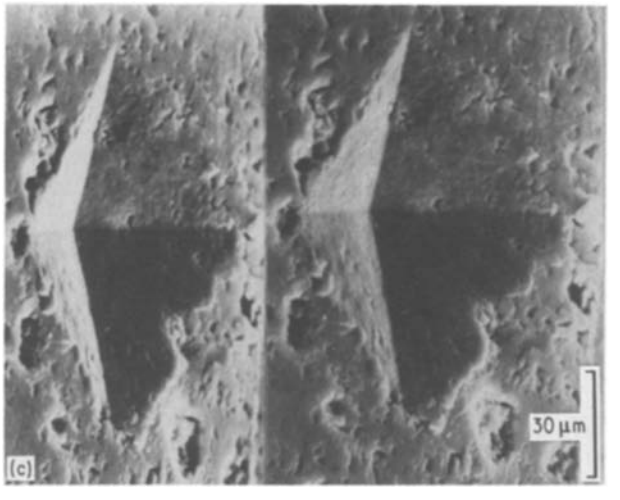

Figure 8 (a) SE and (b) BSE mode SEM images of a 1 kg Vickers indentation made in HX at 800° C. A portion of the indentation is at the upper right-hand corner. (c) A stereo pair of the same indentation taken in the SE mode. Tilt axis is vertical, the left- and right-hand micrographs are at tilts of 45° and 55°, respectively.

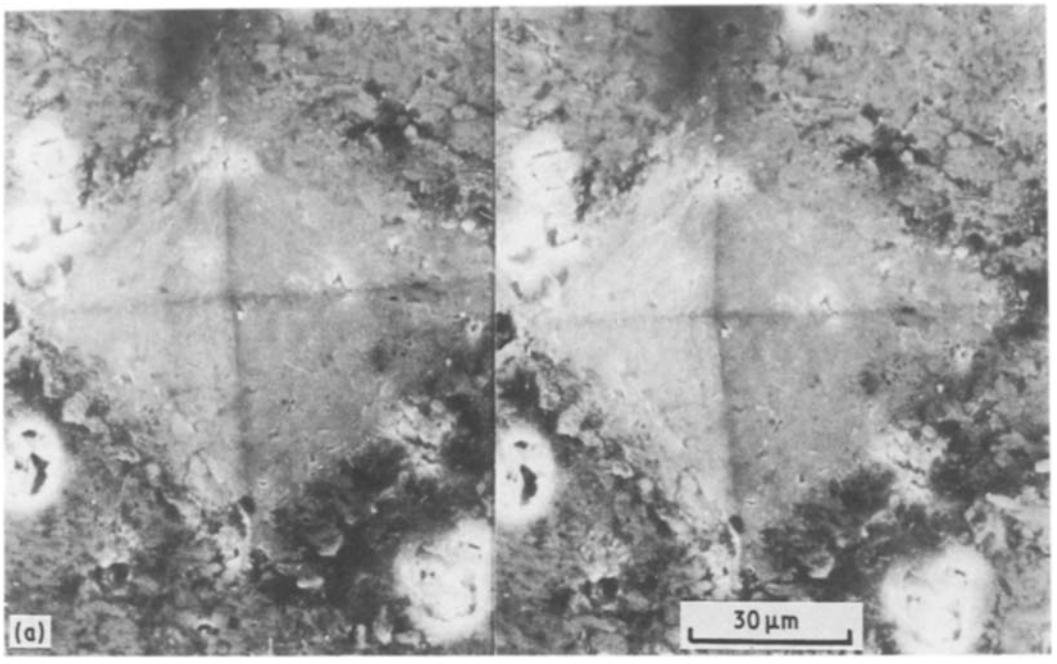

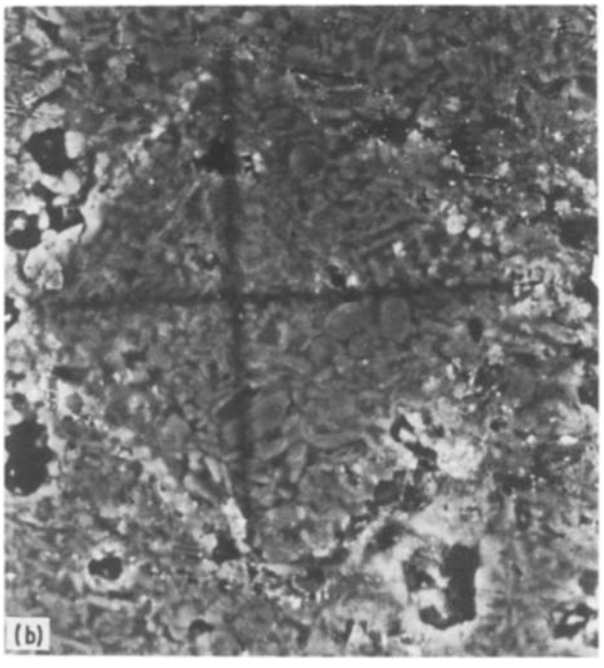

Figure 9 (a) SE mode stereo pair and (b) BSE mode image of a 1 kg Vickers indentation in HX made at 1000° C. Note that the light grey regions in (b) (alumina grains) correspond to those regions standing proud of the facets in (a). In (a) the tilt axis is vertical, left- and right-hand micrographs are at 0° and 10° tilts, respectively.

reason why such extensive fracture is observed at this higher temperature is the extra residual stress from the larger plastic zone size [16]. Another feature of this indentation is the up-lifted region surrounding its edges, seen more clearly in the stereo image of Fig. 8c. This is more characteristic of annealed metals and shows the increase in ductility. Careful examination of the indentation faces in Fig. 8c also shows that they are not smooth (as on room-temperature indenting) but that the alumina grains are slightly proud of the surface.

At still higher temperatures (1000° C, Fig. 9) the grains are more pronounced. The stereo pair and BSE images show that the regions standing proud of the indentation facts are alumina grains, shown as lighter grey in Fig. 9b. At this higher temperature, it is highly likely that the hardness of the crystalline alumina is much greater than that of the siliceous phase. Because elastic recovery is proportional to hardness/stiffness [29, 30] the alumina grains may have recovered more after removal of the load. Alternatively, the glass may have become sufficiently softened at this temperature to flow and fill any sub-indentation porosity.

Severely disrupted (or surface porous) regions were also observed surrounding these higher temperature indentations, shown in Fig. 10. The complementary SE and CL images of RG indented at 1000° C clearly show the extent of this disruption. In Fig. 10a it appears as if the glassy phase has been completely removed from this region leaving surface pores around the grains. The CL image, Fig. 10b, shows that this disrupted region has a suppressed signal, in a similar manner to the indentation itself. If this suppression is due to plastic deformation (affecting the CL response of the alumina grains or of the glass), then this disrupted region may reveal the extent of the plastic zone. If the expanding cavity model of indentation is used (e.g. [19]), then an equation of the form $b \sim a(E/H)^{0.3}$, is obtained; where b is the plastic zone size, a half the indentation diagonal, E Young's modulus and H hardness. The value for E from the manufacturers is $260\,\mathrm{GN\,m^{-2}}$, which from the hardness data should result in $b \sim 300\,\mu\mathrm{m}$, whereas the observed value is $\sim 100\,\mu\mathrm{m}$. However, this assumes a temperature insensitivity to Young's modulus. Because the softening points of glasses is about 600° C (e.g. [31]), this clearly cannot be the case (see also Fig. 9). This lowering of E would make the calculated value tend towards that observed. Thus, high-temperature plastic deformation of the material around the indentation appears to have allowed the softened glass to flow away from the surface. It is clear, therefore, that the decreasing hardness at high temperatures is accompanied by subtle changes in deformation mechanisms mainly attributable to the behaviour of the glass binder phase.

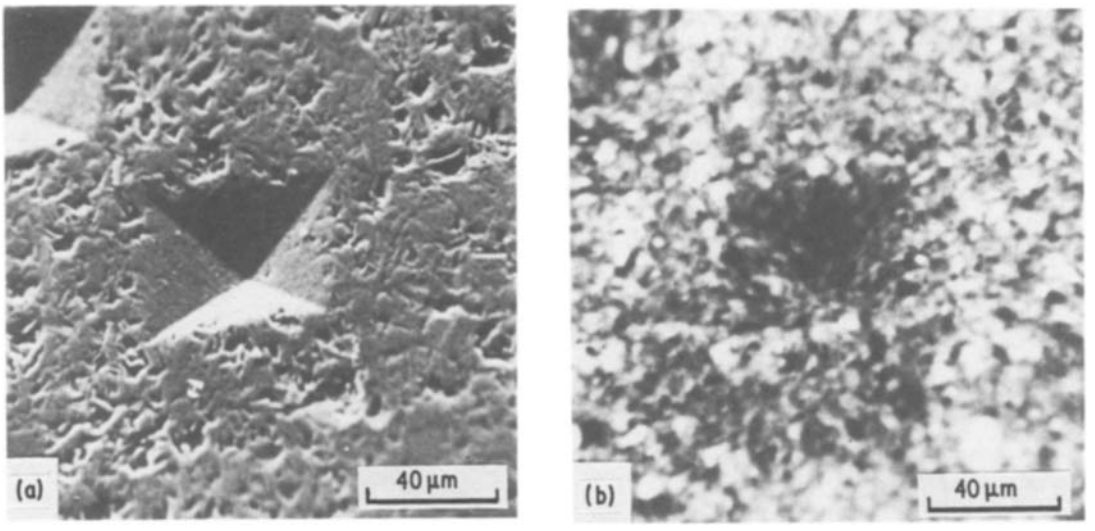

Figure 10 A 1 kg indentation in RG made at 1000° C. (a) SE and (b) panchromatic CL SEM images. The specimen tilt is 45°.

6. Conclusions

The combined hardness dependence on load and temperature has been investigated for four polycrystalline ceramics. Hardness has been shown to be sensitive to indentation size, the hardness increasing with decreasing load for all materials at room temperature but the magnitude of the increase being different for each material. The effect is important in ranking materials by hardness. Further, the actual hardness values, whether at constant load, or constant indentation diagonal are highly sensitive to temperature, such that the ranking of hardness values may again alter with temperature. Such behaviour has been explained jointly in terms of the effect of temperature on the ISE index and changes in viscosity of the grain-boundary phase due to compositional differences. However, many aspects of the deformation mechanisms remain unclear (e.g. the extent of plasticity in the alumina phase).

Scanning electron microscopy has been shown to be particularly useful in highlighting changes in indentation-associated deformation structures as the temperature of the indentation is increased. These include: a granular appearance to the identation itself caused by differential elastic recovery of the grains and/or flow of the glass; those regions surrounding the highest temperature indentations have become severely disrupted with a large proportion of the glassy phase having been removed.

These observations imply that if hardness is used as a materials' selection parameter for use in high-temperature applications, it is clearly insufficient to quote a single "hardness number". The actual values are highly dependent on scale and temperature. In addition, it is necessary to observe the modes and extent of deformation produced around such surface contacts. Furthermore, environment has also been demonstrated to play a role in determining the hardness response and this subject is explored further in a companion paper.

Acknowledgements

J.T.C. wishes to acknowledge a SERC CASE studentship in collaboration with the Fibres Division of ICI plc. The authors wish to thank Professor R.W.K. Honeycombe, FRS, FEng. for the provision of laboratory facilities, and Messrs F. Smith, P. E. Gallant, and R. J. Merigold for their interest in this project and the provision of materials.

References

1. M. M. KRUSCHEV and M. A. BABICHEV, *Russ. Eng. J.* **44** (1964) 43.
2. B. J. HOCKEY, *J. Am. Ceram. Soc.* **54** (1971) 223.
3. *Idem, Proc. Br. Ceram. Soc.* **20** (1972) 95.
4. T. F. PAGE, G. R. SAWYER, O. O. ADEWOYE and J. J. WERT, *ibid.* **26** (1978) 193.
5. A. G. EVANS and D. B. MARSHALL, in "Fundamentals of Friction and Wear of Materials" (American Society of Metals, Metals Park, Ohio, 1981) p. 439.
6. P. M. SARGENT and T. F. PAGE, *Proc. Br. Ceram. Soc.* **26** (1978) 209.
7. M. G. S. NAYLOR and T. F. PAGE, *J. Microscopy* **130** (1982) 345.
8. J. T. CZERNUSZKA and T. F. PAGE, *Proc. Br. Ceram. Soc.* **34** (1984) 145.
9. A. R. C. WESTWOOD, J. S. AHEARN and J. J. MILLS, *Colloids and Surfaces* **2** (1981) 1.
10. K. L. JOHNSON, "Contact Mechanics" (Cambridge University Press, 1985) p. 202.
11. J. T. CZERNUSZKA and T. F. PAGE, *J. Microscopy* **140** (1985) 159.
12. N. K. GIBBS, PhD thesis, University of Cambridge (1982).
13. J. T. CZERNUSZKA, PhD thesis, University of Cambridge (1985).
14. J. T. CZERNUSZKA and T. F. PAGE, *J. Am. Ceram. Soc.* **68** (1985) C196.
15. P. E. GALLANT and R. J. MERIGOLD, *J. Microscopy* **124** (1981) 275.
16. M. G. S. NAYLOR and T. F. PAGE, "ELSI V", Proceedings of the Fifth International Conference of Erosion by Liquid and Solid Impact (Cavendish Laboratory, Cambridge, 1979) Paper 32.
17. P. M. SARGENT, PhD thesis, University of Cambridge (1979).
18. E. MEYER, *Z. Ver. Deutsch. Ing.* **52** (1908) 645.
19. R. HILL, "The Mathematical Theory of Plasticity" (Oxford University Press, 1950) p. 97.
20. T. O. MULHEARN and D. TABOR, *J. Inst. Metals* **89** (1960) 7.
21. M. G. S. NAYLOR, PhD thesis, University of Cambridge (1983).

22. A. G. ATKINS, A. dos S. SILVERIO and D. TABOR, *J. Inst Metals* **94** (1966) 369.
23. H. J. FROST and M. F. ASHBY, "Deformation Mechanism Maps for Ceramics" (Cambridge University Engineering Department, 1981) Ch. 14.
24. D. L. KOHLSTEDT, *J. Mater. Sci.* **8** (1973) 777.
25. H. BUCKLE, in "The Science of Hardness Testing and Its Research Applications" (American Society of Metals, Metals Park, Ohio, 1973) p. 453.
26. D. TABOR, *Rev. Phys. Technol.* **1** (1971) 145.
27. J. H. WESTBROOK and P. J. JORGENSEN, *Trans. Met. Soc. AIME* **233** (1965) 425.
28. D. M. MARSH, *Proc. R. Soc. London* **A279** (1964) 420.
29. B. R. LAWN and V. R. HOWES, *J. Mater. Sci.* **16** (1981) 2745.
30. P. M. SARGENT and T. F. PAGE, *ibid.* **20** (1985) 2388.
31. J. E. STANKWORTH, "Physical Properties of Glass" (Oxford University Press, 1950) p. 158.

Received 24 October 1986
and accepted 22 January 1987